

NJC

Accepted Manuscript



This is an *Accepted Manuscript*, which has been through the Royal Society of Chemistry peer review process and has been accepted for publication.

Accepted Manuscripts are published online shortly after acceptance, before technical editing, formatting and proof reading. Using this free service, authors can make their results available to the community, in citable form, before we publish the edited article. We will replace this *Accepted Manuscript* with the edited and formatted *Advance Article* as soon as it is available.

You can find more information about *Accepted Manuscripts* in the [Information for Authors](#).

Please note that technical editing may introduce minor changes to the text and/or graphics, which may alter content. The journal's standard [Terms & Conditions](#) and the [Ethical guidelines](#) still apply. In no event shall the Royal Society of Chemistry be held responsible for any errors or omissions in this *Accepted Manuscript* or any consequences arising from the use of any information it contains.



www.rsc.org/njc

Water bamboo-derived porous carbons as electrode materials for supercapacitors

Jiangfeng Li, Qingsheng Wu*

Department of Chemistry, Key Laboratory of Yangtze River Water Environment, Ministry of Education, Tongji University, Shanghai 200092, PR China

Abstract:

The microporous carbon materials with specific surface area as high as $2352 \text{ m}^2 \text{ g}^{-1}$ were synthesized by the carbonization of KOH-pretreated partially carbonized water bamboo at $800 \text{ }^\circ\text{C}$ under N_2 atmosphere for supercapacitor application. In particular, the carbon materials synthesized at 2:1 weight ratio of KOH and pre-treated carbon exhibited excellent performance with maximum specific capacitance of 268 F g^{-1} at a current density of 1 A g^{-1} in 6 M KOH electrolyte and retained up to 222 F g^{-1} even at a current density of 10 A g^{-1} . In addition, this material also showed good capacity retention of 97.28 % over 5000 cycles at a current density of 10 A g^{-1} . The excellent electrochemical properties could be due to high specific surface area, abundant pore volume, proper pore size distribution and some oxygen groups.

1. Introduction

Nowadays, the problem of energy shortage is getting more and more serious. Supercapacitors as the new energy storage devices have received amount of attention because of their high power density ($10^3\text{-}10^4 \text{ WKg}^{-1}$), long cycling life ($>10^6$ cycles), high specific capacitance and short charging time ¹⁻⁴. Depending on charge-storage mechanism, supercapacitors can be divided into two classes, i.e.

* Corresponding author. Tel: +86 21 65982620, Fax: +86 21 65981097.

E-mail address: qswu@tongji.edu.cn (Q. Wu).

pseudocapacitors and electrochemical double-layer capacitors (EDLCs) ⁵. In the pseudocapacitor, the capacitance comes from a Faradaic process, indicating that the storage is based on reduction-oxidation reaction ⁶. However, pseudocapacitors suffer from poor electrical conductivity, low power density and lack of stability ^{7, 8}. The capacitance of EDLCs comes from the adsorption of electrolyte ions at electrode and electrolyte interfaces ⁹. Therefore, specific surface area and pore structure of electrodes are two important factors which influence the energy storage of EDLCs ^{10, 11}. In recently years, activated carbon materials, which can be synthesized by template method and chemical/physical activation, have achieved high EDLCs performances ¹²⁻¹⁶. The well-defined pore size distribution, high specific surface area and good crystallinity of activated carbons are keys to exhibiting the electrochemical capacitance performance of such supercapacitors ^{2, 17, 18}.

Recently, biological materials have been attracting much attention in the fabrication of activated carbons for energy applications. Compared with the conventional raw materials (such as petroleum coke, tar pitches and coal), biomasses have three advantages: environmental friendly, low cost and renewables ¹⁹⁻²¹. Several biomass materials such as cornstalks ^{22, 23}, durian shell ²⁴, cherry stone ²⁵, gelatin ²⁶, coffee bean ²⁷, eucalyptus wood saw dust ²⁸, etc are employed to synthesize activated carbons with high specific surface area and porosity. For instance, high performance activated carbon derived from tamarind fruit shell showed a specific capacitance of 412 F g⁻¹ and an energy density of 9.166 Wh Kg⁻¹ in aqueous 1 M H₂SO₄ ¹⁹. Activated carbon materials via high-temperature carbonization of neem (*Azadirachta indica*) dead leaves yield a very high specific capacitance of 400 F g⁻¹ and an energy density of 55 Wh Kg⁻¹ in 1 M H₂SO₄ ²⁹. Zhou et al. successfully utilized natural loofah sponges as precursors to fabricate three-dimensional (3D) porous carbon materials ³⁰.

Water bamboo (*Zizania Latifolia*), a kind of vegetable, is large-scale cultivated along Yangtze

River and the south areas. Despite of being an inexpensive and abundant precursor for producing activated carbon, water bamboo has not been explored in any electrochemical application. In this study, we demonstrate the synthesis of activated carbon materials by the carbonization of KOH-pretreated water bamboo under N₂ atmosphere at high temperature. The porous carbon materials activated by KOH at high temperature can exhibit larger surface areas, abundant micropores and higher content of oxygen groups^{31, 32}. The as-prepared water bamboo-derived carbon (WBC) materials possess a high specific surface area induced by KOH activation.

2. Experimental

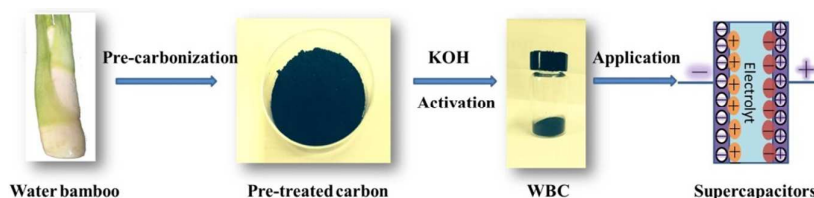
2.1 Materials

The water bamboo was purchased from market in Shanghai. Hydrochloric acid, potassium hydroxide, ethanol, graphite powder were purchased from Shanghai Chemical Reagents Co., Ltd. Deionized water was used throughout the experiments. Pure nitrogen was bought from Shanghai BOC Special Gases Sales Service Co., Ltd. Nickel foil was bought from Shanghai Hongxiang Plant. Polytetrafluoroethylene (PTFE) solution was obtained from Shanghai 3F New Materials Co., Ltd.

2.2 Synthesis of Water bamboo derived porous carbon

Scheme 1 shows the procedure to synthesize the water bamboo derived porous carbon materials. The peeled water bamboo was washed with deionized water, cut into a small debris, and dried at 60 °C in a vacuum oven. The dried debris was preheated at 450 °C for 2 h in a quartz tube furnace under constant N₂ flow. The pre-carbonization materials were ground to powder, mixed with KOH in different proportions, and carbonized in a ceramic crucible from room temperature to 800 °C for 2 h under an nitrogen atmosphere. The carbonized products were immersed in excess 1 M HCl solution, washed several times with hot deionized water, and finally dried at 80 °C. The weight ratio of KOH to

WBC is from 0 to 3 and thus obtained carbons are denoted as WBC-1, WBC-1, WBC-2 and WBC-3, respectively.



Scheme 1 Schematic for the fabrication of porous carbon materials from water bamboo.

2.3 Preparation of the electrodes

To prepare the working electrode, the composite (85 wt %), graphite powder (10 wt %) and PTFE (5 wt %) were mixed homogeneously with deionized water. The mixture was coated onto the nickel foam substrate (1cm×1cm) at 10 MPa and dried at 80 °C in a vacuum oven to remove the deionized water. The active material mass of the electrode is about 1.2 mg. The electrochemical analysis was investigated using the three-electrode cell systems, and a Pt foil and Ag/AgCl electrode were used as the counter and reference electrodes in 6 M KOH electrolyte, respectively.

2.4 Characterization techniques

The prepared materials were investigated by scanning electron microscopy (SEM, Phenom Pro-G2, Netherlands) and transmission electron microscopy (TEM, JEOL JEM-2100, Japan). Powder X-ray diffraction (XRD) was got on Bruker Focus D8 diffract-meter with Cu K α radiation (40 kV, $\lambda=0.15418$ nm) between 10 and 70°. The adsorption amounts were carried out using Micromeritics Tristar 3000 gas adsorption analyzer. The specific surface area was calculated through a single-point Brunauer-Emmett-Teller (BET) method and the pore size distributions were obtained by Barret-Joyner-Halenda (BJH) model from the desorption branch of the isotherms. High temperature was performed with the samples of 10 mg by TPD (temperature programmed desorption) experiments

under a temperature of 850 °C keep 0.5 h (heating rate 10 °C min⁻¹) with a continuous He flow. The evolution of CO and CO₂ was analyzed by mass spectrometer (MS, Hiden HPR20, England). Electrochemical measurements were tested by a CHI 660E electrochemical workstation (ChenHua Corp., Shanghai, China).

3. Results and discussion

3.1 Sample characterization

It is well known that the surface morphology and structure are two important factors influencing the specific capacitance for carbon-based electrochemical materials. Fig. 1A, B and C display the SEM images of the obtained samples, respectively. All the samples exhibit highly irregular surface and abundant porous morphology by activating the pre-carbonized water bamboo with KOH as activator. As depicted in Fig. 1A, the surface of WBC-1 is rough and lax with large pore size more than 5 μm. At KOH/WBC ratio of 2, WBC-2 shows a loose structure with distribution on the surface with massive pores (Fig. 1B). But at KOH/WBC ratio of 3, the number of holes distribution on the surface is reduced seriously, which bring down the specific surface area for ion adsorption and transportation (Fig. 1C). Therefore, the KOH amount should be properly selected to obtain abundant and interconnected porous structure which can significantly enhance the ability of fast charge and mass transport at high current density^{33,34}. The microstructure of WBC-2 was investigated by TEM. As shown in Fig. 1D, WBC-2 has abundant porous structure with the pore sizes less than 2 nm, which provides an effective volume for the absorption of electrolyte ions^{35,36}. Fig. 2 shows the powder XRD spectra of these materials. There are two diffraction peaks clearly observed at 23.6° (graphitic peak) and 44.5° for all WBC samples because of the formation of high levels of in-plane condensation, which should greatly enhance the electrical conductivity³⁷. On closer examination, the crystallinity of WBC-3 is decreased

obviously with the broadening of graphitic peak¹⁵.

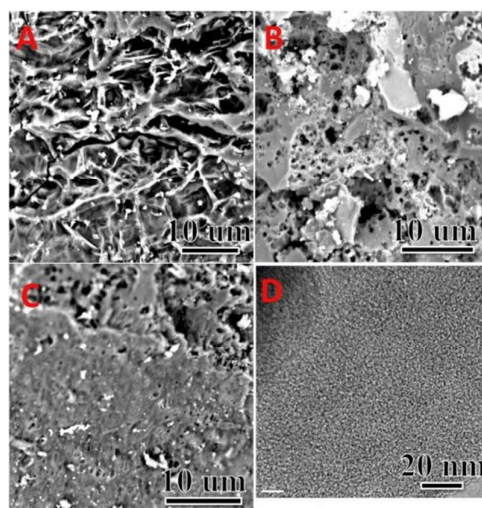


Fig. 1 SEM images of WBC-1 (A), WBC-2 (B) and WBC-3 (C); and TEM image of WBC-2 (D).

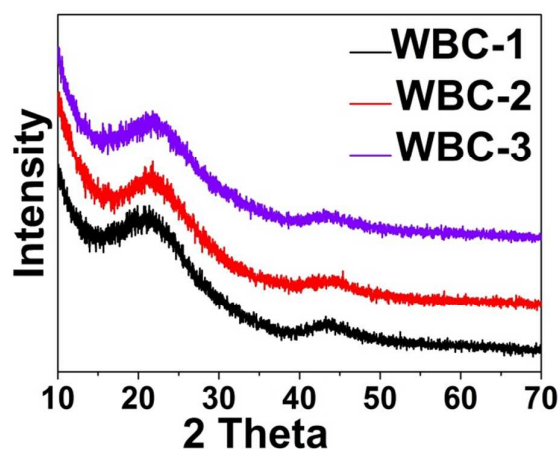
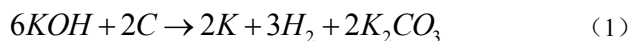


Fig. 2 XRD patterns of samples WBC-1, WBC-2 and WBC-3.

Fig. 3A shows the microstructural characteristics of WBC-1, WBC-2 and WBC-3, analyzed by using nitrogen adsorption/desorption isotherms. The shapes of all samples exhibit a type I isotherm, indicating the microporous character of as-prepared samples^{38, 39}. Fig. 3B shows the pore size distributions of the samples. As depicted in Fig. 3B, these samples have similar pore size distributions, which range from 1.5 to 5 nm. The porous properties of these carbon materials are displayed in Table 1. It can be observed that the BET specific surface areas of KOH-pretreated carbon materials are larger than the direct carbonized materials. At high temperature, KOH can react with carbon to generate H₂,

CO and CO₂, which has contributed to the formation of pores⁴⁰. The reaction mechanism is followed:



The measured BET specific surface areas are 1846, 2352 and 1905 m² g⁻¹ with the pore volumes are 0.95, 1.17 and 0.93 cm³ g⁻¹ for WBC-1, WBC-2 and WBC-3, respectively. It could be seen that WBC-2 had the highest specific surface area with largest micropore volume among all samples. At a higher KOH/WBC ratio, the surface area and micropore volume were reduced badly because of the collapse of small pore walls during the KOH activation process⁴⁰. The samples could obtain an excellent electrochemical performance due to the coexistence of micropores and mesopores. The large specific surface area and high micropore volume of WBC-2 contributes to the transfer and storage of electrolyte ion.

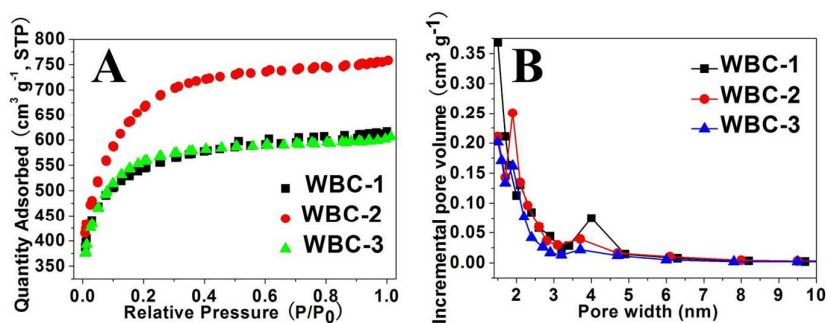


Fig. 3 (A) Nitrogen adsorption/desorption isotherms and (B) pore-size distribution of WBC-1, WBC-2 and WBC-3.

Table 1 Specific surface area and pore characteristics of the obtained samples.

Samples	S _{BET}	S _{langmuir}	V _{pore}	V _{Micro}	D _{aver}
---------	------------------	-----------------------	-------------------	--------------------	-------------------

	[m ² g ⁻¹]	[m ² g ⁻¹]	[cm ³ g ⁻¹]	[cm ³ g ⁻¹]	[nm]
WBC-0	683	926	0.4	0.31	2.3
WBC-1	1846	2539	0.95	0.88	1.93
WBC-2	2352	3308	1.17	1.11	1.99
WBC-3	1905	2639	0.93	0.89	1.84

S_{BET}: BET surface area.

S_{langmuir}: Langmuir surface area.

V_{pore}: Total pore volume.

V_{Micro}: Micropore volume (below 2 nm pore size).

D_{aver}: Average pore size.

3.2 Electrochemical properties

The electrochemical performance of these WBCs was characterized by cyclic voltammetry (CV) analysis in 6 M KOH electrolyte in the range of -0.8 to -0.1 at different scan rates (Fig. 4). As depicted in Fig. 4, all CV curves show almost a rectangular shape at the scan rate of 50 mV s⁻¹. When at the scan rate of 100 mV s⁻¹, the CV curves of these samples are a departure from rectangular shape on account of large ohmic resistances⁴¹. Compared with the CV curves of WBC-1 and WBC-3, the rectangular shape of WBC-2 is a less distorted due to its high surface area and abundant micropores that promoted ion diffusion into inner pores. Among the studied results, the pore structure of WBC-2 is more suitable for ions of electrolytes transfer and adsorption than other two samples, which indicates that WBC-2 was the promising electrode materials for supercapacitors.

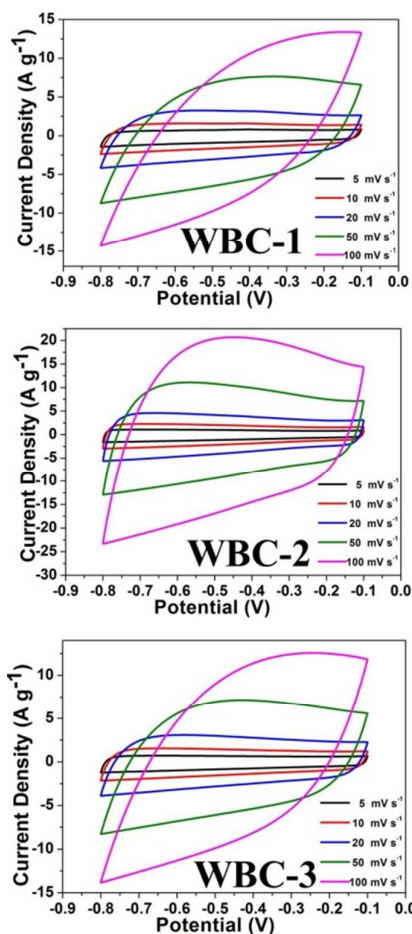


Fig. 4 Cyclic voltammety curves of WBC-1, WBC-2 and WBC-3 at different scan rates.

Galvanostatic charge and discharge technique is an effective method to investigate the performance of these samples-based electrode materials. Fig. 5 shows the galvanostatic charge and discharge curves and specific capacitances of WBC-1, WBC-2 and WBC-3 at different current densities. For quantitative considerations, the specific capacitance is calculated using the following equation:

$$C_s = \frac{I \times \Delta t}{\Delta V \times m} (\text{Fg}^{-1})$$

Where I is the discharge current (A), Δt refers to the discharge time (S), ΔV represents the potential difference (V), and m is the weight (g) of active material. As shown in Fig. 5A, B and C, all the samples have approximately triangular charge/discharge curves and low IR drops at low current

densities of 1 A g^{-1} , indicating these materials had low contact resistance and transported ions quickly⁴². However, all the charge/discharge curves had a little curvature at a low current density of 1 A g^{-1} due to the surface oxygen groups deduced from the activation process³¹. Fig. 6 shows the TPD curves obtained of WBC-0, WBC-1, WBC-2 and WBC-3. As shown in Fig. 6, it can be observed that the amounts of CO of KOH-pretreated carbon materials are larger than the direct carbonized materials. Indicating the carbon materials treated with KOH at high temperature under N_2 atmosphere can produce lots of oxygen-containing functional groups. With the increased amount of KOH, the number of surface oxygen groups is a corresponding increase. This result indicates KOH is helpful to improve the surface oxygen groups of carbon materials. So the high specific capacitance of WBCs could be due to the abundant porosity with high specific surface area and oxygen-containing functional groups, combining double-layer and Faradaic contributions. WBC-1, WBC-2 and WBC-3 showed specific capacitance of 243, 268 and 186 F g^{-1} at the current density of 1 A g^{-1} , respectively. The specific capacitance slightly decreases with the increasing of the current density because of the inadequate time for electrolyte diffusion². However, the specific capacitance of WBC-2 could still maintain 222 F g^{-1} at a high current density of 10 A g^{-1} , while the specific capacitance of WBC-1 and WBC-3 are 144 and 133 F g^{-1} , respectively (Fig. 5D). This result might be due to the high specific surface, the pore size distribution and some surface oxygen groups of the obtained carbon materials which had contributed to transfer electrolyte ions conveniently.

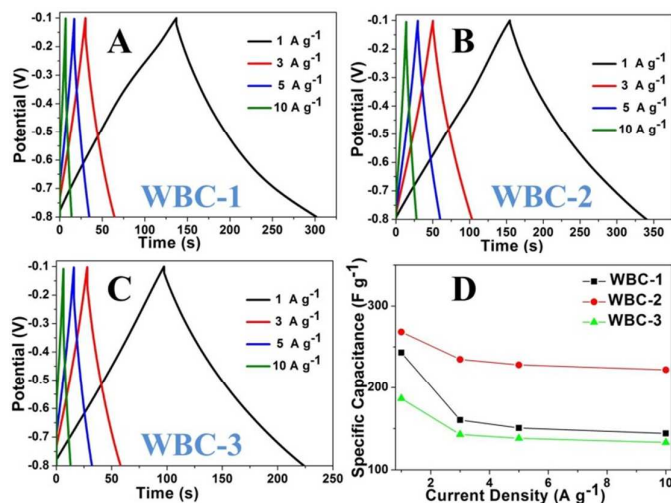


Fig 5 Galvanostatic charge/discharge curves of WBC-1 (A), WBC-2 (B) and WBC-3 (C) at different current densities; Specific capacitances of samples at different current densities (D).

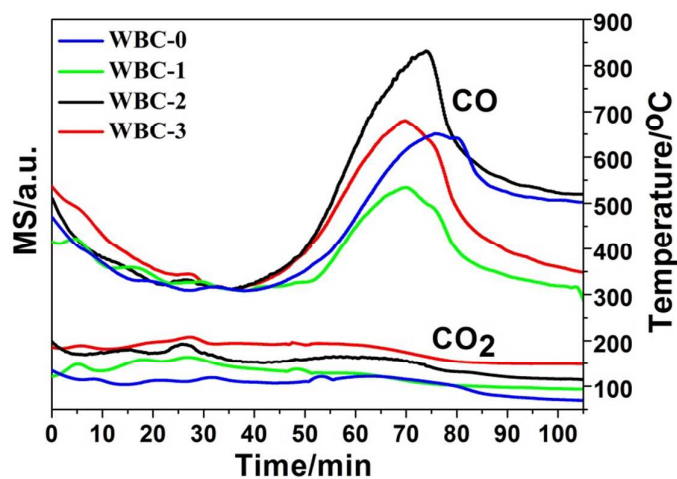


Fig. 6 TPD curves of WBC-0, WBC-1, WBC-2 and WBC-3.

The electrochemical impedance spectroscopy (EIS) is further used to investigate the conductivity of the electrode material. Fig. 7 shows the EIS spectrums of WBC-1, WBC-2 and WBC-3 in the frequency range of 10^{-1} - 10^5 Hz. The theoretical Nyquist plot consists of two regions, (i) an irregular semicircle at high frequency region and (ii) a straight line at low frequency region. As depicted in Fig. 7, the Nyquist plots are almost vertical lines at low frequency region, indicating a typical double-layer charge storage behavior⁴³. The inset in Fig. 7 shows a well-defined semicircle at high frequency region for WBC-2. The Nyquist plot is relatively 45° Warburg region, which is the typical feature of porous

carbon-based electrode^{44,45}. The semicircle at high frequency region is related to the charge transfer resistance (R_{ct}) of the electrode, which is induced by the electroactive surface area of the electrode⁷. The R_{ct} of these samples are all very low, which could improve the ion transmission rate. The reduced R_{ct} of electrode materials is helpful to obtain better rate capability, because R_{ct} is an important factor for fast charge and discharge of supercapacitors⁴⁶.

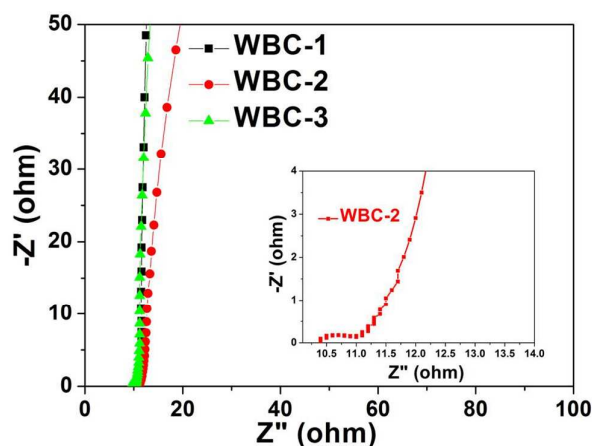


Fig. 7 Nyquist plots in the frequency range from 10^{-1} to 10^5 Hz.

Inset: magnified 9-14 Ω region.

Furthermore, the long-term cycle stability is one of the most crucial factors for supercapacitors. The cyclic stability of WBC-2 was investigated by using galvanostatic charge and discharge technique at a current density of 10 A g^{-1} in 6 M KOH electrolyte for 5000 cycles. Fig. 8 shows the retention of specific capacitance with cycle number. The specific capacitance is reduced obviously between 0 and 1500 cycles and retained up to 2500 cycles. It retains 97.28 % of the initial specific capacitance after 5000 cycles. The dropping in the specific capacitance could be on account of irreversible reaction between electrode and electrolyte⁴⁷. As shown in the inset in Fig. 8, the charging and discharging curve of the sample is completely symmetrical due to the high specific surface area and abundant porosity. This result indicates that WBC-2 electrode shows an excellent stability in cyclic charge/discharge process because of its large specific surface, extensively micropore structure and high

graphitic degree.

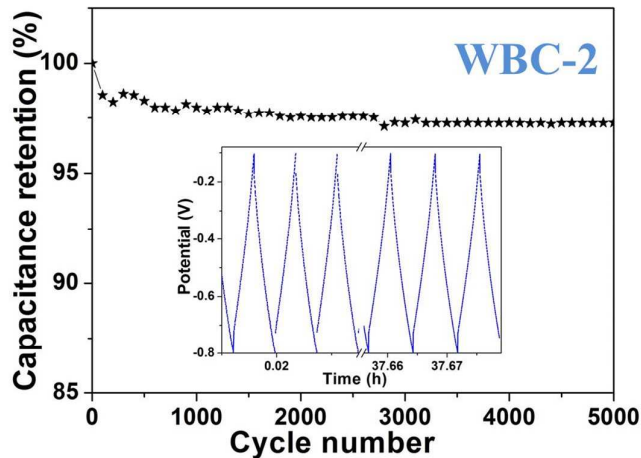


Fig. 8 Cycle stability of WBC-2 at constant current density of 10 A g^{-1} for 5000 cycles.

Inset: galvanostatic in charge/discharge cycles.

4. Conclusion

In summary, three porous carbon materials with tunable microstructures were successfully prepared via carbonization of KOH-pretreated water bamboo through adjusting the ratios of KOH. Based on the experimental results, the porous carbon material synthesized at 2:1 weight ratio of KOH to water bamboo-derived carbon exhibited a high specific capacitance of 268 F g^{-1} in 6 M KOH electrolyte at a current density of 1 A g^{-1} and retained up to 222 F g^{-1} even at a current density of 10 A g^{-1} . In addition, these materials also showed excellent capacity retention of 97.28 % over 5000 cycles at a current density of 10 A g^{-1} . All of the above results demonstrated that the electrochemical properties of water bamboo-derived carbon-based electrodes could be affected by specific surface area, pore size distribution and pore volume. While abundant micropores could increase the specific capacitance area, the existence of mesopores contributed to the efficiently movement of electrolyte ions and obtain high electrochemical performance. The excess amount of KOH could lead to collapse of the micropore volume and the pore structure, which reduced the conductivity of material and further affected its electrochemical performance. In summary, microporous carbon materials can be easily synthesized

from natural plant water bamboo for as an ideal electrode material for supercapacitors.

Acknowledgements

The authors are grateful to the financial support of the National Natural Science Foundation of China (Nos. 21471114, 91122025, 21103127, 21101118), the State Major Research Plan (973) of China (No. 2011CB932404), and the Nano-Foundation of Shanghai in China (No. 11nm0501300).

References:

1. J. P. C. Trigueiro, R. L. Lavall and G. G. Silva, *J Power Sources*, 2014, **256**, 264-273.
2. W. Qian, F. Sun, Y. Xu, L. Qiu, C. Liu, S. Wang and F. Yan, *Energy & Environmental Science*, 2014, **7**, 379-386.
3. Z. Niu, H. Dong, B. Zhu, J. Li, H. H. Hng, W. Zhou, X. Chen and S. Xie, *Adv Mater*, 2013, **25**, 1058-1064.
4. C. Guan, X. Xia, N. Meng, Z. Zeng, X. Cao, C. Soci, H. Zhang and H. J. Fan, *Energy & Environmental Science*, 2012, **5**, 9085-9090.
5. G. Wang, L. Zhang and J. Zhang, *Chem Soc Rev*, 2012, **41**, 797-828.
6. G. A. Snook, P. Kao and A. S. Best, *J Power Sources*, 2011, **196**, 1-12.
7. B. Sethuraman, K. K. Purushothaman and G. Muralidharan, *RSC Advance*, 2014, **4**, 4631-4637.
8. X. Dong, X. Wang, J. Wang, H. Song, X. Li, L. Wang, M. B. Chan-Park, C. M. Li and P. Chen, *Carbon*, 2012, **50**, 4865-4870.
9. G. Wang, L. Zhang and J. Zhang, *Chem Soc Rev*, 2012, **41**, 797-828.
10. S. Kondrat, C. R. Pérez, V. Presser, Y. Gogotsi and A. A. Kornyshev, *Energy & Environmental Science*, 2012, **5**, 6474-6479.
11. R. Kötz and M. Carlen, *Electrochim Acta*, 2000, **45**, 2483-2498.
12. S. Inamdar, H. Choi, P. Wang, M. Y. Song and J. Yu, *Electrochem Commun*, 2013, **30**, 9-12.
13. D. S. Yang, D. Bhattacharjya, S. Inamdar, J. Park and J. S. Yu, *J Am Chem Soc*, 2012, **134**, 16127-16130.
14. L. Zhang, F. Zhang, X. Yang, K. Leng, Y. Huang and Y. Chen, *Small*, 2013, **9**, 1342-1347.
15. D. Bhattacharjya and J. Yu, *J Power Sources*, 2014, **262**, 224-231.
16. X. Xia, H. Liu, L. Shi and Y. He, *J Mater Eng Perform*, 2012, **21**, 1956-1961.
17. W. Huang, H. Zhang, Y. Huang, W. Wang and S. Wei, *Carbon*, 2011, **49**, 838-843.
18. L. Hu and Y. Cui, *Energy & Environmental Science*, 2012, **5**, 6423-6435.
19. S. T. Senthilkumar, R. K. Selvan, J. S. Melo and C. Sanjeeviraja, *ACS Appl Mater Interfaces*, 2013, **5**, 10541-10550.
20. Y. Huang, W. Huang, H. Zhang, W. Wang and S. Wei, *Carbon*, 2011, **49**, 838-843.
21. L. Wei and G. Yushin, *Nano Energy*, 2012, **1**, 552-565.
22. F. Zhang, H. Ma, J. Chen, G. D. Li, Y. Zhang and J. S. Chen, *Bioresour Technol*, 2008, **99**, 4803-4808.
23. L. Wang, G. Mu, C. Tian, L. Sun, W. Zhou, P. Yu, J. Yin and H. Fu, *ChemSusChem*, 2013, **6**, 880-889.
24. T. C. Chandra, M. M. Mirna, J. Sunarso, Y. Sudaryanto and S. Ismadji, *Journal of the Taiwan*

- Institute of Chemical Engineers, 2009, **40**, 457-462.
25. Olivares-Marín M, Fernández J A, Lázaro M J, et al., *Mater Chem Phys*, 2009, **114**, 323-327.
 26. B. Xu, S. Hou, G. Cao, F. Wu and Y. Yang, *J Mater Chem*, 2012, **22**, 1988-1993.
 27. C. Huang, T. Sun and D. Hulicova-Jurcakova, *ChemSusChem*, 2013, **6**, 2330-2339.
 28. L. Wei, M. Sevilla, A. B. Fuertes, R. Mokaya and G. Yushin, *Advanced Energy Materials*, 2011, **1**, 356-361.
 29. M. Biswal, A. Banerjee, M. Deo and S. Ogale, *Energy & Environmental Science*, 2013, **6**, 1249-1259.
 30. Y. Yuan, S. Zhou, Y. Liu and J. Tang, *Environ Sci Technol*, 2013, **47**, 14525-14532.
 31. V. Barranco, M. A. Lillo-Rodenas, A. Linares-Solano, A. Oya, F. Pico, J. Iban ez, F. Agullo-Rueda, J. M. Amarilla and J. M. Rojo, *The Journal of Physical Chemistry C*, 2010, **114**, 10302-10307.
 32. J. Zhang, L. Jin, J. Cheng and H. Hu, *Carbon*, 2013, **55**, 221-232.
 33. X. He, Y. Geng, J. Qiu, M. Zheng, X. Zhang and H. Shui, *Energ Fuel*, 2010, **24**, 3603-3609.
 34. V. Ruiz and A. G. Pandolfo, *J Power Sources*, 2011, **196**, 7816-7822.
 35. Z. Li, Z. Xu, X. Tan, H. Wang, C. M. Holt, T. Stephenson, B. C. Olsen and D. Mitlin, *Energy & Environmental Science*, 2013, **6**, 871-878.
 36. D. Feng, Y. Lv, Z. Wu, Y. Dou, L. Han, Z. Sun, Y. Xia, G. Zheng and D. Zhao, *J Am Chem Soc*, 2011, **133**, 15148-15156.
 37. J. P. Paraknowitsch, J. Zhang, D. Su, A. Thomas and M. Antonietti, *Adv Mater*, 2010, **22**, 87-92.
 38. V. Ruiz, C. Blanco, M. Granda, R. Menéndez and R. Santamaría, *J Electroanal Chem*, 2008, **618**, 17-23.
 39. X. Jin, M. Zhang, Y. Wu, J. Zhang and J. Mu, *Ind Crop Prod*, 2013, **43**, 617-622.
 40. J. Wang and S. Kaskel, *J Mater Chem*, 2012, **22**, 23710-23725.
 41. Q. Cheng, J. Tang, J. Ma, H. Zhang, N. Shinya and L. C. Qin, *Phys Chem Chem Phys*, 2011, **13**, 17615-17624.
 42. T. E. Rufford, D. Hulicova-Jurcakova, K. Khosla, Z. Zhu and G. Q. Lu, *J Power Sources*, 2010, **195**, 912-918.
 43. P. Guo, Y. Gu, Z. Lei, Y. Cui and X. S. Zhao, *Micropor Mesopor Mat*, 2012, **156**, 176-180.
 44. Q. Wu, Y. Xu, Z. Yao, A. Liu and G. Shi, *ACS Nano*, 2010, **4**, 1963-1970.
 45. K. Wang, Q. Meng, Y. Zhang, Z. Wei and M. Miao, *Adv Mater*, 2013, **25**, 1494-1498.
 46. D. Liu, Q. Wang, L. Qiao, F. Li, D. Wang, Z. Yang and D. He, *J Mater Chem*, 2012, **22**, 483-487.
 47. Y. Wang and Y. Xia, *J Electrochem Soc*, 2006, **153**, A450-A454.